Zeitschrift: IABSE publications = Mémoires AIPC = IVBH Abhandlungen
Band: 33 (1973)

Artikel: Analysis of folded plate and cylindrical shell roofs
Autor: Hrennikoff, A.
DOI: https://doi.org/10.5169/seals-25633

Nutzungsbedingungen
Die ETH-Bibliothek ist die Anbieterin der digitalisierten Zeitschriften auf E-Periodica. Sie besitzt keine Urheberrechte an den Zeitschriften und ist nicht verantwortlich für deren Inhalte. Die Rechte liegen in der Regel bei den Herausgebern beziehungsweise den externen Rechteinhabern. Das Veröffentlichen von Bildern in Print- und Online-Publikationen sowie auf Social Media-Kanälen oder Webseiten ist nur mit vorheriger Genehmigung der Rechteinhaber erlaubt. Mehr erfahren

Conditions d'utilisation
L'ETH Library est le fournisseur des revues numérisées. Elle ne détient aucun droit d'auteur sur les revues et n'est pas responsable de leur contenu. En règle générale, les droits sont détenus par les éditeurs ou les détenteurs de droits externes. La reproduction d'images dans des publications imprimées ou en ligne ainsi que sur des canaux de médias sociaux ou des sites web n'est autorisée qu'avec l'accord préalable des détenteurs des droits. En savoir plus

Terms of use
The ETH Library is the provider of the digitised journals. It does not own any copyrights to the journals and is not responsible for their content. The rights usually lie with the publishers or the external rights holders. Publishing images in print and online publications, as well as on social media channels or websites, is only permitted with the prior consent of the rights holders. Find out more

Download PDF: 20.10.2025

ETH-Bibliothek Zürich, E-Periodica, https://www.e-periodica.ch

Analysis of Folded Plate and Cylindrical Shell Roofs

Analyse de toits en plaques pliées et en forme de coques cylindriques

Analyse gefalteter Platten- und zylindrischer Schalendächer

A. HRENNIKOFF
Sc. D., Research Professor, Emeritus, of Civil Engineering, University of British Columbia, Vancouver, B. C., Canada

General

Folded plate roof, as exemplified in Fig. 1, is a structure consisting of several rectangular strips resembling closely the cylindrical or barrel shape roof. Both are supported by cross diaphragms or walls, and in some cases also by the vertical edge beams. In barrel roofs the latter may be either distinct from the barrel (Fig. 2), or be merging into it gradually (Fig. 3).

The analysis of folded plates, as of cylindrical shells, may be carried out by the displacement method using models composed of numerous flat rectangular finite elements or cells. There is an essential distinction in the actions of these two types of structures: the nodes of the folded plate situated along the inter-fold ridges cannot rotate about the axes normal to the ridge lines. This peculiarity results in a substantial complication of the solution, calling for the use of a special iteration procedure.

The method of solution is illustrated on a particular example of folded plate roof, and its results are compared with those of two closely resembling it barrel roofs provided with edge beams.

Finite Element Models of Cylindrical and Folded Plate Roofs

The model of cylindrical shell is a polygonal surface made up of a number of flat rectangular elements inscribed into the actual surface of the shell. The elements are endowed with the direct stress and flexural stiffnesses. Cells of this kind have nodes with five degrees of freedom: three displacements along the coordinate axes and two rotations about the axes in the plane of the cell.

Rotation about the axis normal to this plane is impossible in the prototype, and so it is suppressed in the model. With four nodes in the cell its stiffness matrix has the size 20×20.

The model of folded plate is constructed by subdividing the folds into cells of suitable size, with some of their nodes falling on the inter-fold ridges, and the others away from them.

It is easy to see that the ridge nodes have four degrees of freedom, three displacements and only one rotation about the ridge line L. Consider as an example a rotation vector (an angle) θ of the node 1 in Fig. 4. This vector is equivalent to two components θ' and θ''. The node 1 in the cell B is obviously capable of rotation θ, but the same node in the cell A can undergo only the rotation θ' and not θ''. Since the node belongs to both cells, it cannot rotate about any axis other than L along the ridge line.

The four movements of the ridge nodes generate five force and moment components at the cell nodes including the moments about the axes Y_L or Y_R in the directions of the folds. Thus a rectangular cell adjacent to the ridge, with two nodes on it, has stiffness matrix with 20 rows and only 18 columns.

It is appropriate to mention at this point, that the conclusion just reached with regard to the nature of possible rotations of the ridge nodes in a folded plate model does not apply to the shell model in spite of the similarity in appearance of the two models. The angularity of the cell to cell connection in the barrel roof model results from the finite size of cells. As their size diminishes the angularity decreases toward zero. In the folded plate model the angularity remains constant, no matter how small are the cells.

Solution of Cylindrical Shell Model

The method is described in Ref. [1], and it consists of computer solution of the equation

$$[K_m]\{\delta_0\} = \{P_0\}. \tag{1}$$

Here $\{\delta_0\}$ is the vector of the nodal displacements of the model produced by the load vector $\{P_0\}$, all loads of which are applied at the nodes. Both these vectors are referred to shell coordinates. $[K_m]$ is the stiffness matrix of the model combined of 20×20 cell stiffness matrices. The cells may be either of the bar (framework) type, or of the no-bar type. Only the former will be used here.

The cell matrices are expressed first with reference to the cell axes X, Y, Z, – matrix $[K]$, and then they are transformed to the shell axes L, T, R (Fig. 5) – matrix $[K_0]$. This is imperative for solution of Eq. (1). The axes L at all nodes are the same as the axes X. The T and R axes are different along the circumference, and they are inclined to the axes Y and Z at the angles $+\frac{1}{2}\beta$ and $-\frac{1}{2}\beta$ on the two sides of the cell. In the cell axes the matrices $[K]$

consist of two uncoupled parts, the 8×8 plane stress part and the 12×12 flexure part. These are given in Ref. [2]. For convenience the nodal forces corresponding to unit movements of the node 1 are stated in Tables 1 and 2. The rest of the terms follow from the conditions of symmetry.

Table 1. Stiffness Matrix Terms – Plane Stress – Rectangular Bar Cell

Action 1, $\Delta x_1 = 1$ 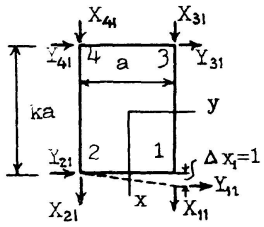		Action 2, $\Delta y_1 = 1$ 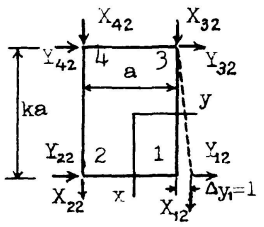	
$X_{11} = \frac{4+k^2(1-3\mu)}{8k(1-\mu^2)} Et$	$Y_{11} = \frac{1}{8(1-\mu)} Et$	$X_{12} = \frac{1}{8(1-\mu)} Et$	$Y_{12} = \frac{1-3\mu+4k^2}{8k(1-\mu^2)} Et$
$X_{21} = -\frac{(1-3\mu)k}{8(1-\mu^2)} Et$	$Y_{21} = \frac{1-3\mu}{8(1-\mu^2)} Et$	$X_{22} = -\frac{1-3\mu}{8(1-\mu^2)} Et$	$Y_{22} = \frac{1+\mu-4k^2}{8k(1-\mu^2)} Et$
$X_{31} = \frac{-4+k^2(1+\mu)}{8k(1-\mu^2)} Et$	$Y_{31} = -\frac{1-3\mu}{8(1-\mu^2)} Et$	$X_{32} = \frac{1-3\mu}{8(1-\mu^2)} Et$	$Y_{32} = -\frac{1-3\mu}{8k(1-\mu^2)} Et$
$X_{41} = -\frac{k}{8(1-\mu)} Et$	$Y_{41} = -\frac{1}{8(1-\mu)} Et$	$X_{42} = -\frac{1}{8(1-\mu)} Et$	$Y_{42} = \frac{1}{8k(1-\mu^2)} Et$

Transformation of the cell matrix $[K]$ into the shell matrix $[K_0]$ is done by the relation

$$[K_0] = [M]^T [K][M]. \tag{2}$$

The transformation matrix $[M]$ is defined by the expression

$$\{\delta\} = [M]\{\delta_0\}. \tag{3}$$

The displacement vectors $\{\delta\}$ and $\{\delta_0\}$, respectively in cell and shell coordinates, are described explicitly by the expressions

$$\{\delta\}^T = (\Delta x_1, \Delta y_1, \Delta z_1, \theta_1^x, \theta_1^y, \Delta x_2, \Delta y_2 \ldots \theta_3^x, \theta_3^y, \Delta x_4, \Delta y_4, \Delta z_4, \theta_4^x, \theta_4^y), \tag{4}$$

$$\{\delta_0\}^T = (u_1, v_1, w_1, \theta_1^L, \theta_1^T, u_2, v_2 \ldots \theta_3^L, \theta_3^T, u_4, v_4, w_4, \theta_4^L, \theta_4^T). \tag{5}$$

Numbering of the cell nodes 1 to 4 is given in Fig. 5. The same $[M]$ relates also the nodal load components $\{P\}$ and $\{P_0\}$.

The 20×20 transformation matrix $[M]$ may be written

$$[M] = \begin{bmatrix} [m_r] & 0 & 0 & 0 \\ 0 & [m_l] & 0 & 0 \\ 0 & 0 & [m_r] & 0 \\ 0 & 0 & 0 & [m_l] \end{bmatrix}_{20\times 20}. \tag{6}$$

Here the 5×5 submatrices $[m_r]$ and $[m_l]$ are as follows:

$$[m_r] = \begin{bmatrix} 1 & 0 & 0 & 0 & 0 \\ 0 & \operatorname{Cos}\frac{1}{2}\beta & \operatorname{Sin}\frac{1}{2}\beta & 0 & 0 \\ 0 & -\operatorname{Sin}\frac{1}{2}\beta & \operatorname{Cos}\frac{1}{2}\beta & 0 & 0 \\ 0 & 0 & 0 & 1 & 0 \\ 0 & 0 & 0 & 0 & \operatorname{Cos}\frac{1}{2}\beta \end{bmatrix} \tag{7}$$

and

$$[m_l] = [m_r]^T. \tag{8}$$

Table 2. Nodal Forces and Moments. Rectangular Bar Cell.

Action 3, $\Delta z_1 = 1$	Action 4, $\theta_1^x = 1$	Action 5, $\theta_1^y = 1$
$Z_{13} = 6\left(k - \frac{\mu}{k} + \frac{1}{k^3}\right)\frac{L}{a}$	$Z_{14} = -3kL$	$Z_{15} = \frac{3}{k^2}L$
$Z_{23} = -6\left(k - \frac{\mu}{k}\right)\frac{L}{a}$	$Z_{23} = 3\left(k - \frac{\mu}{k}\right)L$	$Z_{25} = 0$
$Z_{33} = -6\left(\frac{1}{k^3} - \frac{\mu}{k}\right)\frac{L}{a}$	$Z_{34} = 0$	$Z_{35} = -3\left(\frac{1}{k^2} - \mu\right)L$
$Z_{43} = -\frac{6\mu}{k}\frac{L}{a}$	$Z_{44} = \frac{3\mu}{k}L$	$Z_{45} = -3\mu L$
$m_{13}^x = -3kL$	$m_{14}^x = 2\left(k + \frac{1-3\mu}{4k}\right)aL$	$m_{15}^x = -2\mu aL$
$m_{23}^x = -3\left(k - \frac{\mu}{k}\right)L$	$m_{24}^x = \left(k - \frac{\mu}{k}\right)aL$	$m_{25}^x = 0$
$m_{33}^x = 0$	$m_{34}^x = -\frac{1-3\mu}{2k}aL$	$m_{35}^x = 0$
$m_{43}^x = -\frac{\mu}{k}L$	$m_{44}^x = \frac{\mu}{k}aL$	$m_{45}^x = -\mu aL$
$m_{13}^y = \frac{3}{k^3}L$	$m_{14}^y = -2\mu aL$	$m_{15}^y = 2\left(\frac{1}{k} + \frac{(1-3\mu)k}{4}\right)aL$
$m_{23}^y = 0$	$m_{24}^y = 0$	$m_{25}^y = -\frac{(1-3\mu)k}{2}aL$
$m_{33}^y = 3\left(\frac{1}{k^2} - \mu\right)L$	$m_{34}^y = 0$	$m_{35}^y = \left(\frac{1}{k} - \mu k\right)aL$
$m_{43}^y = 3\mu L$	$m_{44}^y = -\mu aL$	$m_{45}^y = \mu kaL$
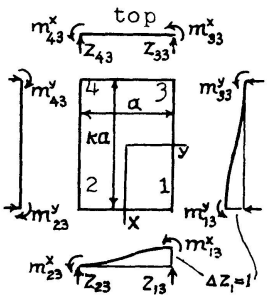	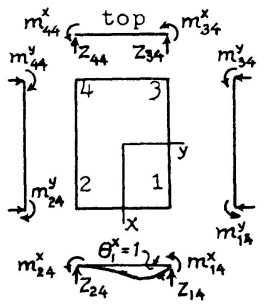	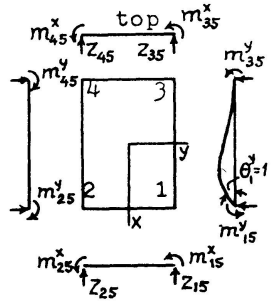

$$L = \frac{E\,t^3}{12\,(1-\mu^2)\,a}$$

Generation of stiffness matrices in shell coordinates should be preferably left to computer.

After the Eq. (1) is solved for the displacement vector $\{\delta_0\}$ in shell coordinates, the displacements in the individual cells are transformed to cell coordinates by Eq. (3), and the nodal forces and moments in all cells are found using Eq. (1). By spreading these over the tributary areas of the model the stresses in the prototype are found.

Solution of Folded Plate Model

The relation of the structure axes L, T, R to the cell axes X, Y, Z at the ridge nodes (Fig. 6) is much the same as in the shell model. The angle β represents here the angle between the adjacent folds. At the nodes on the flat parts of the folds the structure axes and the cell axes are the same.

As was explained earlier, the ridge nodes do not rotate about T axis, and their other nodal movements result in moments about this axis. The displacement vector $\{\delta_0\}$ contains only four movements at each of the ridge nodes and five at all other nodes. The Eq. (1) is solved for these. The structure subjected to these movements remains unbalanced at the ridge nodes with regard to the moments about T axis, and this calls for a special operation. For reasons which will be made clear later, these moments or, more correctly, the moments other than M^L, will be referred to the axes lying in the plane of the cell, i. e. to Y_L in the cells A on the left of the ridge, and Y_R in the cells B on the right.

Conversion of the stiffness matrices of cells, situated along the ridge, from cell to structure coordinates is subject to Eq. (2), but the transformation matrix $[M]$ is different from the one used with shell models. Furthermore, it is different for the cells A and B.

For the cells A:
$$[M_A] = \begin{bmatrix} [1] & 0 & 0 & 0 \\ 0 & [m_{l0}] & 0 & 0 \\ 0 & 0 & [1] & 0 \\ 0 & 0 & 0 & [m_{l0}] \end{bmatrix}_{20\times 20}. \tag{6a}$$

For the cells B:
$$[M_B] = \begin{bmatrix} [m_{r0}] & 0 & 0 & 0 \\ 0 & [1] & 0 & 0 \\ 0 & 0 & [m_{r0}] & 0 \\ 0 & 0 & 0 & [1] \end{bmatrix}_{20\times 20}. \tag{6b}$$

Here
$$|m_{r0}| = \begin{bmatrix} 1 & 0 & 0 & 0 & 0 \\ 0 & \operatorname{Cos}\frac{1}{2}\beta & \operatorname{Sin}\frac{1}{2}\beta & 0 & 0 \\ 0 & -\operatorname{Sin}\frac{1}{2}\beta & \operatorname{Cos}\frac{1}{2}\beta & 0 & 0 \\ 0 & 0 & 0 & 1 & 0 \\ 0 & 0 & 0 & 0 & 1 \end{bmatrix}, \tag{7a}$$

$$[m_{l0}] = [m_{r0}]^T. \tag{8a}$$

The symbol [1] signifies 5×5 diagonal unit matrix.

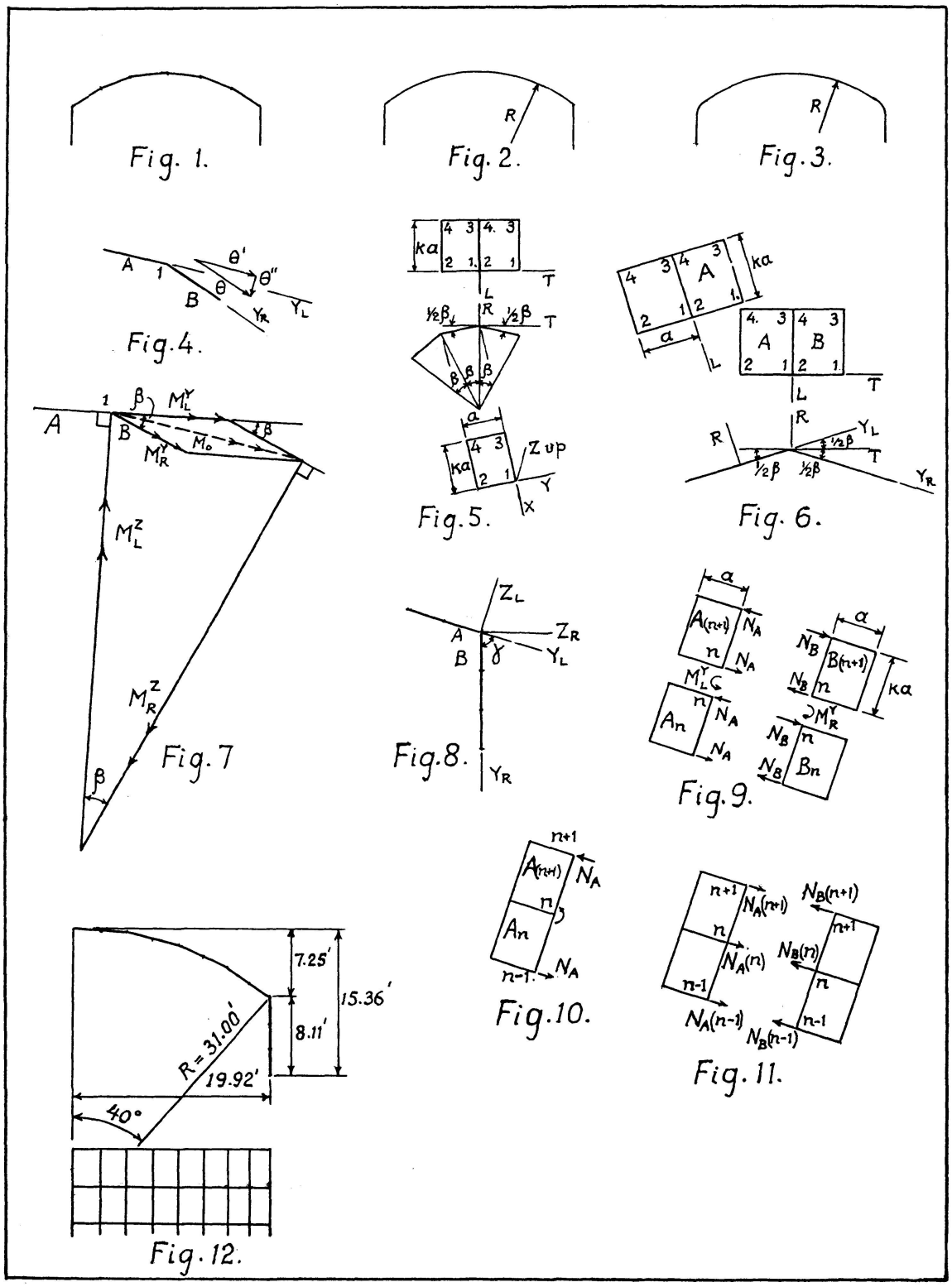

In cells with no nodes on the ridge lines the stiffness matrices in cell and structure coordinates are the same. Should the cell extend for the full width of the fold from ridge line to ridge line, the Eqs. (6), (7) and (8), used for the shell models hold also here, except that the fifth row, fifth column term in the submatrices $[m_r]$ and $[m_l]$ should be unity in place of $\operatorname{Cos} \frac{1}{2}\beta$.

Complete solution of a folded plate problem is carried out in several steps. The first step, the determination of nodal displacements by Eq. (1), ignoring the lack of moment equilibrium, and subsequent determination of the unbalanced nodal moments has already been described. Let M_L^Y and M_R^Y (Fig. 7) be the vectors of these unbalanced moments, each of which comes from two cells adjacent to the node in question. Equilibrium of these is effected by development of resistances following the most rigid route available to them in the structure, namely by the way of the moments M_L^Z and M_R^Z, which are normal to the directions Y_L and Y_R respectively. Being the equilibrants, these moments close the vector polygon. The principle invoked here is an aspect of that of least work. Its common example is the action of a bridge truss with riveted joints. The load carried by it follows the most rigid route by the way of direct stresses, with very little of it left to the secondary or flexural stresses.

The moments M_L^Z and M_R^Z may be expressed by trigonometry from the vector diagram as follows:

$$\begin{aligned} M_L^Z &= M_L^Y \operatorname{Cot}\beta + M_R^Y \operatorname{Cosec}\beta, \\ M_R^Z &= M_L^Y \operatorname{Cosec}\beta + M_R^Y \operatorname{Cot}\beta. \end{aligned} \tag{9}$$

The positive signs of these moments are the ones in Fig. 7.

The roof-edge beam ridge (Fig. 8) merits a few further remarks, although it is substantially the same as the other ridges. It is convenient to make the structure axes at its nodes coincident with the cell axes of the beam X, Y_R, Z_R. Then the stiffness matrices of the beam cells B need no transformation from the cell axes, and the transformations of the roof cells A are carried out in the same manner as of the other ridge cells A by the Eqs. (2), (6a), (7a) and (8a), except that the angle γ (Fig. 8) is used in place of $\frac{1}{2}\beta$ in Eq. (7a). The moments M_L^Z and M_R^Z are found by Eqs. (9) with replacement by γ of the angles β in these equations.

Consider now a ridge node n and its unbalanced moments M_L^Z and M_R^Z shown by circular arrows in Fig. 9. It is legitimate to assume that each such moment is produced in equal parts in the cells A or B adjacent to this node (call them A_n and A_{n+1} or B_n and B_{n+1}), and that each of these moments is formed by a pair of oppositely directed transverse forces N_A or N_B applied at the nodes, as shown. The force contributions at the node n of the two cells cancel each other. Thus the unbalanced moment M_L^Y at any node n is balanced by the oppositely directed forces

$$N_A = \frac{M_L^Z(n)}{2ka} \tag{10}$$

applied at the nodes $(n-1)$ and $(n+1)$ in Fig. 10. A similar expression holds for the force N_B. The symbol (n) in the numerator of the expression signifies the location of the moment M_L^Z. It follows from this analysis, that the trans-

verse forces at the node n are contributed by moments at the nodes $(n-1)$ and $(n+1)$. They are (Fig. 11)

$$N_A(n) = \frac{1}{2ka}[M_L^Z(n+1) - M_L^Z(n-1)],$$
$$N_B(n) = \frac{1}{2ka}[M_R^Z(n+1) - M_R^Z(n-1)]. \tag{11}$$

The forces $N_A(n)$ and $N_B(n)$ in these expressions represent the residue of the loads acting on the structure, remaining still unbalanced after completion of the first step of solution of the displacement problem. Now in the second step the model is analyzed again under the action of these loads N without involvement of the actual applied loads considered in the first step. The new solution yields among its results the new moments M_L^Y and M_R^Y, whose equilibrants, the new M_L^Z and M_R^Z, are converted again into the new forces N to be treated the same as their predecessors. The iteration procedure described here is expected to end quickly. The complete solution of the problem is given by the combination of the results of all steps.

With cells of finite size the final results exhibit some unusual peculiarity – an absence of exact balance of forces both at the ridge nodes and in the cells adjacent to the ridges. The reason for this is not difficult to see. The unbalanced moments M_L^Y and M_R^Y belonging to the node n are not balanced at this node, because the forces N developing the balancing moments M_L^Z and M_R^Z are applied not at the node n, but at the nodes $(n-1)$ and $(n+1)$. Furthermore, the moment M_L^Y could not be equilibrated by the corresponding moment M_L^Z even if it were applied at the node n because its magnitude does not depend on M_L^Y alone, but also on M_R^Y. As the cells are reduced to a very fine size, and the stress conditions in the adjoining units become nearly uniform, the joints approach balance, and so do the pairs of the oppositly located cells A and B, taken together. Actually, however, a quite good balance is attained even when the cells are fairly large.

Structures Analyzed

The theory is applied to an example of folded plate roof, with vertical edge beams on the sides, supported by the end diaphragms. The folds, two cells wide, are inscribed into a circular curve of $R = 31'$, and the total internal angle of 80°. The structure (Fig. 12) 77.5′ long and 39.84′ wide between the edge beams, is symmetrical about two vertical planes. Its model is formed of $2.703' \times 3.875'$ bar cells of aspect ratio $k = 1.4355$, with 20 cells along the length and 22 laterally, of which number three cells on each side belong to the edge beams.

The load is made up of the weight of reinforced concrete in the roof and

the edge beams $3^3/_4''$ thick, amounting to 47 lbs. per sq. ft. of surface, and of snow load of 25 lbs. per sq. ft. of horizontal projection. The material is assumed to have uniform elastic properties with $E = 3\,(10)^6$ lbs./sq. ft. and $\mu = 0.2$.

The results of analysis of this structure, described as No. 1, are compared with those of two shell structures, resembling it closely in shape. The model of the first of these (structure No. 2) has the same number and size of cells, and is illustrated by the same Fig. 12, its only difference from the folded roof being the location of all roof nodes on the circumscribed cylindrical surface. The last or No. 3 structure (Fig. 13) is characterized by shape with gradual transition from the roof to the edge beam, and while the number and size of its cells is still the same as in the other two structures, its width and over-all height are about 2% different from them. The three structures are compared with regard to deflections, thrusts and moments in some significant locations.

Deflections

These are compared at the nodes between the mid-span and the end diaphragm as follows: vertical deflections along the crown line, vertical deflections along the bottom of the edge beam and the horizontal deflections in the same locations on the edge beam.

All these deflections present smooth parabolic curves (Fig. 14) of the type $y = k x^n$ with the order n of the parabola varying between 1.65 and 2.07. The corresponding ordinates in the three structures differ somewhat in magnitude, as indicated in Fig. 14, not always in the same sequence. Their greatest ordinates and the values of the parameter n are stated in Table 3. The greatest difference in deflections between the three structures is found in horizontal deflections, the structure No. 3 having only 0.7 of the value of the folded plate. The vertical deflections are much closer. This agreement in deflections is

Table 3. Deflections of Three Roof Structures.

	No. 1 Folded Plate with Edge Beams			No. 2 Barrel Roof with Edge Beams		No. 3 Barrel Roof Merged Smoothly into Edge Beams	
	δ inch	n	r	δ inch	n	δ inch	n
Vertical, Crown Line	0.216	1.65	1.25	0.208	1.74	0.222	2.07
Vert., Bot'm Edge Beam	0.0555	1.71	0.67	0.0611	1.76	0.0546	2.06
Horiz., Bot', Edge Beam	0.561	1.76	1.57	0.492	1.73	0.390	1.93

rather curious, when one considers the difference in analytical procedure employed in solutions.

Another result worthy of being pointed out is the substantial difference in deflections of the folded plate structure between the final values and the ones following the first step of the solution procedure prior to balancing the ridge moments M^Y. The initial and final deflections stand in a nearly constant ratio all along the span; these ratios $r = \delta_f/\delta_i$ are also stated in Table 3. The fact that the ratio r is much greater than one, shows, that it is incorrect to leave the ridge moments unbalanced, as suggested by some investigators (3).

Thrusts

The lengthwise thrusts in the prototype structures on the planes normal to L axis are found by dividing the relevant nodal forces by the tributary

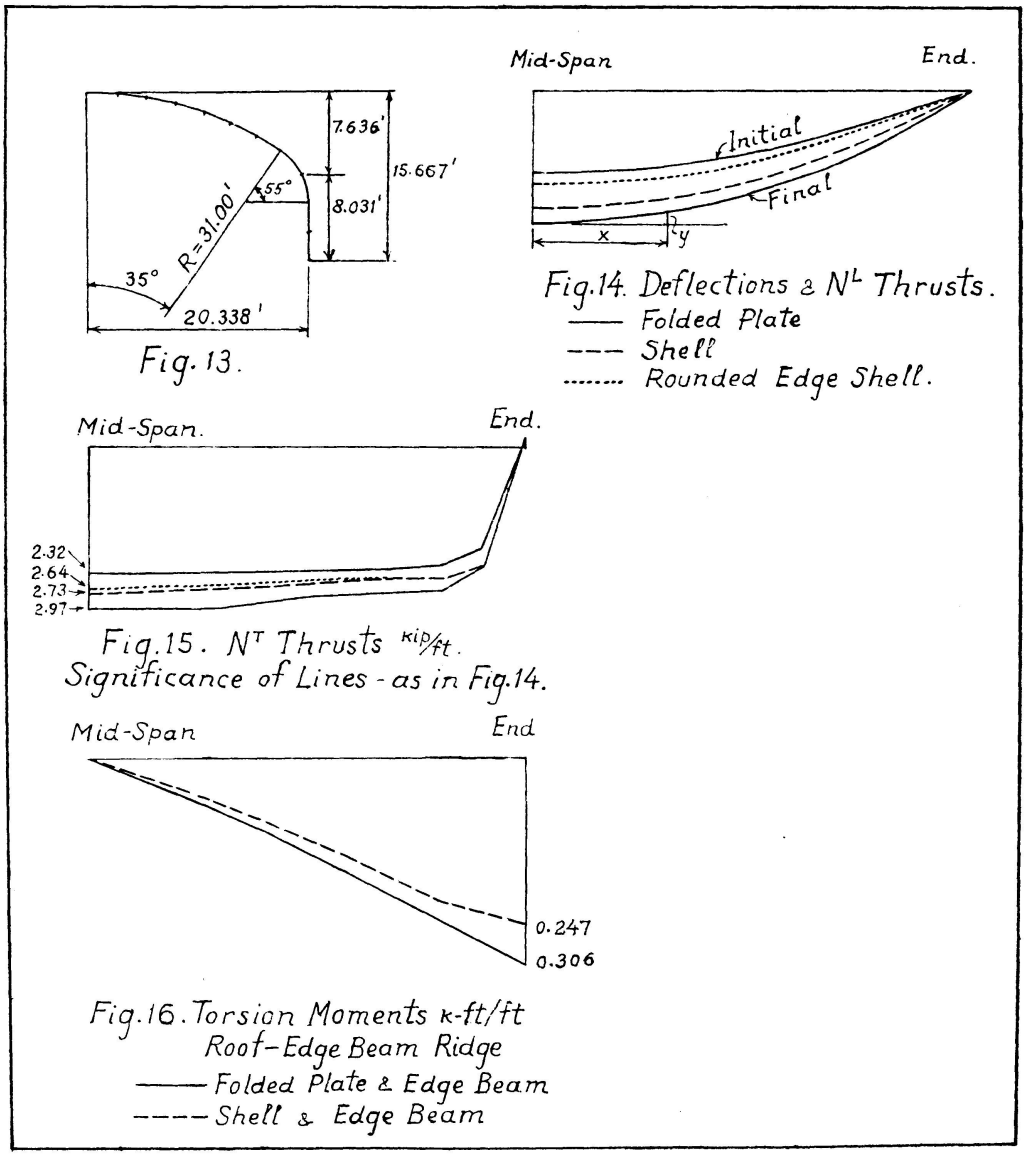

Fig. 13.

Fig. 14. Deflections & N^L Thrusts.
—— Folded Plate
--- Shell
..... Rounded Edge Shell.

Fig. 15. N^T Thrusts kip/ft.
Significance of Lines - as in Fig. 14.

Fig. 16. Torsion Moments k-ft/ft
Roof-Edge Beam Ridge
—— Folded Plate & Edge Beam
---- Shell & Edge Beam

lengths. This means, that along the crown line and the ridge junction of the roof and the edge beam the L nodal forces in the two cells adjacent to the node are divided by the width of the cell 2.703′. On the underside of the edge beam the cell nodal force is divided by $\frac{1}{2}$(2.703′), and at the same time multiplied by 1.09, to allow for the change in the lever arm to the neutral axis of the section from the edge beam to the centre of the triangularly distributed thrust area.

The diagrams of these N^L forces are also parabolic in shape, and they resemble closely the deflections diagrams of Table 3. The Table 4, in which they are assembled, contains the maximum values of thrusts, the orders of the parabolae n and the ratios r between the final thrust values and the ones prior to balancing the moments on the ridges.

Table 4. N^L Thrusts of Three Roof Structures

	No. 1 Folded Plate with Edge Beams			No. 2 Barrel Roof with Edge Beams		No. 3 Barrel Roof Merged Smoothly into Edge Beams	
	N^L max. kip/ft.	n	r	N^L max. kip/ft.	n	N^L max. kip/ft.	n
On Crown Line	−14.50	1.72	1.28	−13.36	1.70	−13.11	1.83
Roof-Edge B. Junction	11.37	2.45	1.43	10.30	2.50	8.91	2.25
Bot. Edge of Edge Beam	18.30	1.95	1.01	17.90	1.90	18.15	1.89

The thrusts along the crown line in T direction are not distributed parabolically as the L thrusts. They are nearly equal over several nodes near the mid-span (Fig. 15), and then they decrease towards the end supports first slowly and then sharply. The ordinates of the curves in the three structures are still more or less proportional to each other.

Bending Moments

These are investigated on L and T (or Y) planes along the crown and along the roof-edge beam ridge. The crown moments M^T appear in the form of parabolic curves of the same general shape in all three structures. The results are stated in Table 5, arranged as Table 3. From this table it may be observed, that the moments M^T in the structure No. 2 are only half as great, and in the structure No. 3 one third as great as in the folded plate roof. The

Table 5. M^T Bending Moments Along the Crown

Structure	M^T max. k. ft./ft.	n	r
No. 1 Folded Plate	0.537	2.90	1.475
No. 2 Shell and E. B.	0.283	2.50	
No. 3 Rounded E. B.	0.187	2.88	

latter moments are about $1\frac{1}{2}$ times greater than their incomplete values present just after the step 1 of the solution.

The M^T moments in the folded plate structure along the roof-edge beam ridge do not vary a great deal, and their maximum moment value is only about a quarter of 0.537 k-ft./ft. crown moment in Table 5. In the structure No. 2, also subject to two-step iteration analysis, this moment is still smaller by some 20%. In the structure No. 3, devoid of the ridge, the moments M^T in the area under consideration are very small.

The bending moments M^L along the ridge nodes, unlike the moments M^T, cannot be found by the method of nodal concentrations in view of the existence of the earlier described special equilibrium conditions. However, a quite simple different method is available for this purpose. With the ridge nodes undergoing no rotations about T or Y axes, the basic relation of elasticity between the moments on the two perpendicular planes becomes $M^L = \mu M^T$, making M^L proportional to the known moment M^T with the coefficient of proportionality μ.

Torsion Moments

Direct determination of torsional moments M_{yx} at the ridge from the nodal moment concentrations in the planes T or Y is impossible because of the special condition of unbalance of these moments. On the other hand, it is felt, that the moments M_{xy} may be found in the usual manner from the nodal concentrations in the plane L, ignoring the angularity of the roof-beam junction, which is not believed to affect M_{xy} significantly. The moment M_{yx} is then found by the relation of elasticity $M_{yx} = -M_{xy}$. With the roof and the edge beam cells being of the same size, the M_{xy} moments are equal on both sides of the ridge.

The diagrams of torsional moments M_{xy} along the line of the roof-edge beam nodes in the structures 1 and 2 are comparable in shape, as may be seen from Fig. 16. Beginning with zero values at mid-span, the torques increase to maximum at the supports, following the lines not too far different from straight, with the values of torques in the structure 1 being some 15 to 20% greater than in the structure 2.

Conclusions

1. The presence of angular ridges in the folded plate structures complicates considerably the displacement method of their analysis, in view of inability of the ridge nodes to rotate about the axes perpendicular to the ridge, thus leaving unbalanced the moments about these axes. Development of a suitable iteration procedure for equilibration of these moments represents an original contribution of this paper.

2. The method is applied to a particular vertically loaded folded plate roof structure, called No. 1, provided with longitudinal vertical edge beams. Two other similarly loaded structures, No. 2 and No. 3, covering equal areas, are analyzed for comparison, the No. 2 structure being a barrel roof with the same edge beams, and No. 3 – a similar barrel roof curving gradually into the edge beams.

3. Deflections and stresses of different kinds, namely, normal stresses in longitudinal and transverse directions, and flexural moments and torques in L and T planes along both the crown and the ridge line, are determined and compared in all three structures. Structure No. 3 has the smallest stresses and deflections, followed by No. 2, with No. 1 developing the greatest stresses and deflections in all but one comparatively unimportant case of deflection. Judging by these examples, barrel roofs, not necessarily of constant radius across them, have definite advantage in stresses and deflections over the folded plates.

4. The apparent general inferiority of folded plates in comparison with shells is subject to one qualification applicable to thin metallic shells. Such shells, unlike comparatively thick reinforced concrete structures, may fail by instability, and their resistance to failure of this kind is definitely improved by the presence of interfold ridges.

Acknowledgement

The present investigation was carried out with financial assistance of the National Research Council of Canada, whose contribution is gratefully acknowledged.

Notation

A, B	cells on left and right.
E	modulus of elasticity.
$[K]$, $[K_0]$	cell stiffness matrices in cell and structure coordinates.
$[K_m]$	stiffness matrix of whole model.
L, T, R	structure axes and coordinates.

$[M], [M_A], [M_B], [M]^T$	transformation matrices and transpose matrix.
M^L, M^T	bending moment at the node on L and T planes.
$M_L^Y, M_R^Y, M_L^Z, M_R^Z$	nodal moments on Y or Z planes on left and right sides.
$M_x, M_y, M_n, M_n', M_{12}, M_{13}, T_{12}, T_{13}$	nodal moments, as defined.
M_{xy}, M_{yx}	torsion moments.
N, N_A, N_B	nodal forces in Y direction.
N^L, N^T	normal thrusts in structures on L and T planes.
$\{P\}, \{P_0\}$	vectors of nodal forces referred to cell and structure axes.
R	radius of structure.
X, Y, Z	cell coordinate axes.
Y_L, Y_R, Z_L, Z_R	axes on left and right of node.
X, Y, Z with two subscripts	terms of cell stiffness matrix.
a	cell dimension along X axis.
k	cell aspect ratio.
$[m_{l0}], [m_{r0}], [m_l], [m_r]$	submatrices.
m^x, m^y with two subscripts	terms of cell stiffness matrix.
n	parameter of parabola.
r	ratio of final and initial displacements.
t	thickness of shell or folded plate.
u, v, w with subscripts	nodal displacements in structure coordinates.
x, y, z	coordinates referred to cell axes.
$\Delta x, \Delta y, \Delta z$ with subscripts	nodal displacements referred to cell axes.
β	external angle between adjacent cells or folds.
γ	external angle between roof and edge beam at the ridge.
$\{\delta\}, \{\delta_0\}$	node displacement vectors in cell and structure coordinates.
μ	Poisson's ratio.
θ, θ', θ''	angle vectors.
θ^x, θ^y with subscripts	nodal rotations, referred to cell axes.
θ^L, θ^T with subscripts	nodal rotations, referred to structure axes.

References

1. A. Hrennikoff and S. S. Tezcan: Analysis of Cylindrical Shells by the Finite Element Method. International Association for Shell Structures, Symposium, Leningrad U.S.S.R., 1966.

2. A. Hrennikoff, C. I. Mathew and Rajan Sen: Stability of Cylindrical Shells by the Use of Rectangular Bar Cells. International Association for Shell Structures, Symposium, Honolulu, Hawaii, U.S.A., October 1971.
3. C. Meyer and A. C. Scordelis: Analysis of Curved Folded Plate Structures. Jour. of Structural Div., Proceedings of A.S.C.E., October 1971.

Summary

The finite element method, making use of rectangular bar cells, is applied to deflection and stress analysis of cylindrical shell and folded plates structures. The latter require the use of a special iteration procedure in view of inability of the ridge nodes to rotate about axes other than parallel to the ridge lines on which they are situated. The application of the method is illustrated on the examples of three structures. The results show that folded plates are inferior to cylindrical shells, closely resembling them in shape, both in stresses and deflections.

Résumé

La méthode des éléments finis se servant de cellules de barres rectangulaires est appliquée à l'analyse de déflexions et de tensions de coques cylindriques et de structures en plaques pliées. Ces dernières demandent l'emploi d'un procédé d'itération spécial, étant donnée l'incapacité des points de jonction de tourner autour des axes non parallèles aux lignes des sommets du toit où elles sont situées. L'application de la méthode est illustrée par l'exemple de trois structures. Les résultats montrent que des plaques pliées sont inférieures aux coques cylindriques quant aux tensions et déflexions bien que dans la forme elles leurs rassemblent beaucoup.

Zusammenfassung

Die Methode der endlichen Elemente wird unter Verwendung rechteckiger Stabzellenelemente auf die Biegungs- und Spannungsberechnung zylindrischer Schalen und gefalteter Plattentragwerke angewendet. Die letzteren erfordern den Gebrauch eines besonderen Iterationsverfahrens und zwar im Hinblick auf die Unfähigkeit der Knotenpunkte, um andere Achsen zu rotieren als solche parallel zu den Faltenlinien, in denen sie liegen. Die Anwendung der Methode wird an Beispielen von 3 Bauten erläutert. Die Ergebnisse zeigen, dass gefaltete Platten zylindrischen Schalen hinsichtlich Beanspruchung und Durchbiegung unterlegen sind, obwohl sie ihnen in der Form sehr ähnlich sind.

Leere Seite
Blank page
Page vide